ORIGINAL ARTICLE

Generation of microdroplets in T-junction devices by pulsed fluid flow: Simulation studies

K. Sripadaraja[1] · M. N. Satyanarayan[1] · G. Umesh[1]

Abstract

We present an investigation on microdroplet generation and trapping by simulation of two-phase liquid flow in a T-junction microfluidic device using the CFD package in ANSYS. In this study, the flowrate of the continuous phase liquid is kept constant, whereas that of the dispersed phase liquid is pulsed between zero and 0.1 μl/s. We have observed a new regime of droplet generation, wherein droplets are generated in pairs. When the pulse duration is high (on-time = 6.5 ms), a pair of droplets are generated per pulse when a surfactant is added at a concentration of 1% or more. For smaller pulse duration (3.25 ms), a single droplet is generated per pulse irrespective of the concentration of the surfactant. Smaller droplets can be generated by reducing the width of the side channel in the device. We have also observed that the inclusion of a small pinhole ahead of the microwell ensures trapping of the droplets in the microwell over a larger range of flowrates indicating the positive role of the pinhole in the trapping process.

Keywords Droplet microfluidics · Droplet-on-demand · Pulsed flow · Droplet trapping · Volume of fluid (VOF)

Introduction

Droplet microfluidics has advanced in the last two decades to a stage, wherein programmed generation of monodispersed droplets, of nanoliter volumes, at the desired rate has become possible. The interest in this field is driven by a variety of novel applications such as protein crystallization (Zheng et al. 2004), measurement of blood clotting time using anticoagulant drugs (Song et al. 2006), drug discovery (Brouzes et al. 2009), single-cell analysis (Kemna et al. 2012), encapsulation of microfibers in microdroplets for food processing, cosmetics, and pharmaceutical products (Nunes et al. 2013), synthesis of microcapsules (Kong et al. 2013; Datta et al. 2014; Lee et al. 2016), polymer chain reaction methods for DNA amplification (Zhang and Jiang 2016), encapsulating multicell organism (Beneyton et al. 2016). Droplet generation has been achieved using microfluidic devices of mainly three types, viz. T-junctions (Li et al. 2012), cross junction (Seo et al. 2007), and co-

flow (Hong and Wang 2007). In all these devices, the droplet generation involves the flow of two immiscible liquids. The primary liquid is called the continuous phase liquid whose viscosity is μ_c and it flows in the main channel with flowrate Q_c. The second liquid is called the dispersed phase liquid whose viscosity is μ_d. It flows through the side channel with a flowrate Q_d. Interactions of the two immiscible liquids in the flow channel lead to droplet formation by either squeezing, dripping, or jetting mechanism. The mechanism that will dominate in any experiment will depend on parameters such as flowrates of the two liquids (Yan et al. 2012), the viscosity ratio ($\lambda = \mu_d/\mu_c$) (Nekouei and Vanapalli 2017), the aspect ratio of the channels (Gupta and Kumar 2010; Gupta et al. 2014), and interfacial tension between the two fluids (Peng et al. 2011). For practical applications, it is important to generate droplets of the same volume. T-junction-based microfluidic devices have been widely studied as they are simple to fabricate and analyze (Sontti and Atta 2017). In the present investigation, we have investigated droplet generation in a T-junction device.

The mechanism of microdroplet generation depends largely on the value of capillary number C_a, which is the ratio of shear stress to the interfacial tension. In their

✉ K. Sripadaraja
  sripadaraja@gmail.com

[1] Department of Physics, National Institute of Technology,
  Karnataka, Surathkal, Mangalore, Karnataka 575025, India

seminal paper, Thorsen et al. (2001) showed that the droplet generation in T-junction devices for $C_a > 0.01$ is dominated by shear stress overcoming the interfacial tension, and the mechanism is called dripping. For $C_a < 0.01$, the droplets are formed due to the squeezing mechanism (Menech et al. 2008; Liu and Zhang 2009) wherein, the pressure buildup in the plug formed by the dispersed phase liquid dominates. C_a values close to 0.01 constitute a transition regime in which both mechanisms play a role. Glawdel et al. (Glawdel and Ren 2012) have proposed a model to predict the droplet size and droplet generation frequency in the transition regime and validated it experimentally. The aspect ratio of the flow channels and the ratio of the viscosities of the two liquids also play a role in droplet formation (Christopher et al. 2008). Droplet generation by adopting novel channel geometries has been reported (Carrier et al. 2014; Liu et al. 2018; Li et al. 2019). It is seen that the droplet volume reduces with a decrease in interfacial tension and an increase in contact angle (Bashir et al. 2011). Generation of droplets at high frequencies (more than 1000 droplets per minute), which are required for some applications, has also been investigated (Collins et al. 2015).

All these studies summarized above refer to droplet generation by the steady flow of the two immiscible liquids, wherein a steady stream of microdroplets are generated. Many applications require droplets of constant volume to be generated at a prescribed rate, which ensures the optimum use of liquids, thereby reducing the costs. Such techniques are called droplet on demand (DoD). One way of achieving DoD is by pulsing the flow of dispersed phase liquid, while the continuous phase liquid flowrate is kept constant. In DoD devices, the flow of the dispersed phase liquid is controlled by using commercially available microvalves at the inlet of the side channel through which it flows into the device. In the first DoD device, demonstrated by Lin et al. in (2008), the generation of droplets of different volumes were achieved by controlling the inlet pressure of the dispersed phase liquid and the duration for which the valve was kept open (Lin and Su 2008). In such devices, both pneumatic- and electromagnetic-based microvalves were used (Churski et al. 2010). Piezoelectric microvalves have been used to produce droplets of nanoliter to picoliter volumes at a frequency ranging from 20 Hz to 400 Hz (Jakiela et al. 2014). The microvalves are usually operated in the pulsed mode by adopting standard pulse waveforms such as rectangular, triangular, and sinusoidal functions of time. In a recent study, it has been shown that the use of rectangular voltage waveforms for operating the microvalves leads to better control of the droplet volume (Qian et al. 2019).

An important application of droplet microfluidics is the generation of multiple droplets and merging them at the desired stage. This is of relevance to studies on chemical/biochemical reactions. In a device having two T-junctions, two droplets can be generated separately, each having different reagents. One such device was developed to produce two droplets containing DNA and DNA markers to perform fluorescence imaging on the merged droplet (Guo et al. 2010). Similar experiments were carried out to perform mass spectroscopy on merged droplets of myoglobin and pepsin (Sun et al. 2013). A device with four T-junctions was realized and used to produce four droplets of different reagents in the same device (Zec et al. 2012). Experiments on single-cell pairing were carried out using multiple droplets with mineral oil as the continuous phase liquid (Babahosseini et al. 2019). Simulation studies have been carried out on a microfluidic device with multiple T-junctions to optimize their performance (Tangen et al. 2015). These studies have shown that the droplet volume and the generation frequency may be controlled by the proper choice of the pulse waveform for the valve and the inlet pressure.

It is often required to eliminate the coalescence of droplets in microfluidic devices or in the vial in which the droplets are collected for further investigations. The addition of surfactants to either of the two liquids is known to reduce the interfacial tension between the liquids, thereby preventing the coalescence of droplets (Tadros 2013). The change in the interfacial tension, due to the addition of SDS (sodium dodecyl sulfate) or Tween 20 as a surfactant was estimated experimentally in a study on the generation of water droplets in silicone oil, and an analytical model was developed for determining the change in interfacial tension (Wehking et al. 2014). It has been shown by simulation studies that the distribution of surfactant on the surface of the droplets is nonuniform and evolves with time (Bastani et al. 2018; Riaud et al. 2018). It is shown that, during the droplet generation process, the adsorption of surfactant occurs initially at the front end of the interface of the two liquids as it expands into the main channel and gradually spreads over the entire droplet just before it is pinched-off. The addition of a surfactant has also been shown to lead to an increase in the frequency of droplet generation (Chen et al. 2016). Very recently, the generation of water droplets in FC-40, using surfactants such as 1H,1H,2H,2H-perfluoro-1decanol and PEG-Krytox, was studied. It was observed that the flow velocity of the droplet increased by 25%, which was exploited to control the distance between the droplets and also for an on-demand merging of two droplets. The use of surfactants such as Picosurf-1 in a DoD device has been shown to stabilize the generated droplets and improve the wetting of the main channel walls of the DoD device (Totlani et al. 2020).

The trapping of microdroplets in an array makes it convenient for chemical/biological investigations. Several

mechanisms have been explored in order to trap the droplet in a microwell based on the surface energy of the micro-droplet (Dangla et al. 2011), Laplace pressure (Simon et al. 2012) and hydrodynamic-based trapping (Wang et al. 2009). In the case of surface energy-based trapping mechanism, a pinhole is made in the microchannel, which is much smaller than the droplet (Dangla et al. 2011; Abbyad et al. 2011). At flowrates below the threshold value, the droplet anchors to the pinhole. The droplet motion experiences a force proportional to the gradient of surface energy as it deforms due to the pinhole. When the surface energy gradient is dominant over the hydrodynamic drag force, the droplet anchors to the pinhole. The threshold velocity at which larger droplet anchors to the pinhole was also determined (Nagel et al. 2014) with various viscous media (Amselem et al. 2015). This mechanism has also been studied using the Lattice Boltzmann method (Liu and Zhang 2017). This study demonstrates that anchoring efficiency increases with an increase in the diameter of the pinhole.

In this paper, we report on simulation studies on droplet generation by pulsing the flow of dispersed phase liquid on two T-junction devices whose side-channel widths are 50 μm and 25 μm. The width of the main channel is 100 μm in both the devices. The flowrate of the dispersed phase liquid (water) is switched between 0.1 μl/s (flow state) and 0 μl/s (no flow state), while that of the continuous phase liquid (mineral oil) is kept constant at 0.2 μl/s. The flowrate profile is chosen to be a rectangular pulse waveform. The temporal variation of the pressure within the water column in the side channel is investigated for two different pulse widths and two different pulse duty cycles. These studies were repeated for droplet generation using Span80 as surfactant dissolved in mineral oil. We also investigate trapping droplets of length 80 μm and 40 μm. The influence of a circular pinhole near the microwell is investigated by varying its depth and diameter. We also consider the effect of using surfactant on the trapping of droplets.

In the simulation results presented in this paper on droplet generation, we have concentrated on the pressure variations within the two liquids at a point close to the T-junction. This gives us an insight into the droplet formation mechanisms. Previous studies have shown that the difference between the pressure within the two liquids is larger in the squeezing regime than in the dripping and jetting regimes (Yang et al. 2013; Garstecki et al. 2006). The pressure variations in the dispersed phase liquid from 22 kPa to 12 kPa, during the droplet generation, are seen to lead to a corresponding decrease in the interfacial tension from 0.06 mN/m to 0.015 mN/m (Chen et al. 2016). It has

been shown that periodic droplet generation results from an interplay between the interfacial tension and viscous drag acting at the interface (Li et al. 2012). Variations of droplet length for capillary number ranging from 0.001 to 10 have been studied, using the lattice Boltzmann method, for both Newtonian and non-Newtonian fluids, and validated experimentally (Chiarello et al. 2017). Further, it has been shown that for a fixed value of C_a, the droplets can be produced in the squeezing regime for $Q = Q_d/Q_c > 2$ and in the dripping regime for $Q < 0.5$ (Loizou et al. 2018). These studies indicate that microdroplet generation and trapping is a complex process and depends on several parameters. Therefore, a good understanding of droplet generation and trapping mechanism requires detailed simulation studies and subsequent validation by suitable experiments.

Microfluidic device model

The T-junction device is schematically shown in Fig. 1a, b. The two channels have a rectangular cross section. The channel plate has a T-shaped microchannel of a rectangular cross section. The well plate has a well diameter of 200 μm and depth of 200 μm and a pinhole depth of 40 μm. The separation between the pinhole and the well is 20 μm. The channel plate is placed on the well plate and clamped together tightly to obtain the complete microfluidic device.

The fluid equations used in the simulation are listed below. The continuity equation for an incompressible fluid is given by Batchelor (2000)

$$\nabla \cdot (\rho_{\text{avg}} \vec{U}) = 0 \tag{1}$$

And for the motion of the fluid is given by,

$$\frac{\partial (\rho_{\text{avg}} \vec{U})}{\partial t} + \nabla \cdot (\rho_{\text{avg}} \vec{U} \vec{U}) = -\nabla P + \nabla \cdot \overline{\tau} + \overrightarrow{F_{\text{SF}}} \tag{2}$$

where $\vec{U}$, ρ_{avg}, P, $\bar{\tau}$ and $\vec{F}_{\text{SF}}$ are velocity, density (averaged), pressure, stress tensor and surface tension force, respectively, for the fluid. In the case of Newtonian liquids, the shear stress is relative and is proportional to the rate of strain tensor $\dot{\gamma}$ which is represented as,

$$\overline{\tau} = \dot{\gamma} \eta_{\text{avg}} = \eta_{\text{avg}} (\nabla \vec{U} + \nabla \vec{U}^T) \tag{3}$$

where η_{avg} is the viscosity (averaged). In a system involving two immiscible liquids, the density (averaged) and viscosity (averaged) are defined in terms of the fractional volume (V_f) such as oil (V_o) and water (V_w) as follows (Ranade 2019).

$$\rho_{\text{avg}} = V_0 \rho_o + (1 - V_w) \rho_w \tag{4}$$
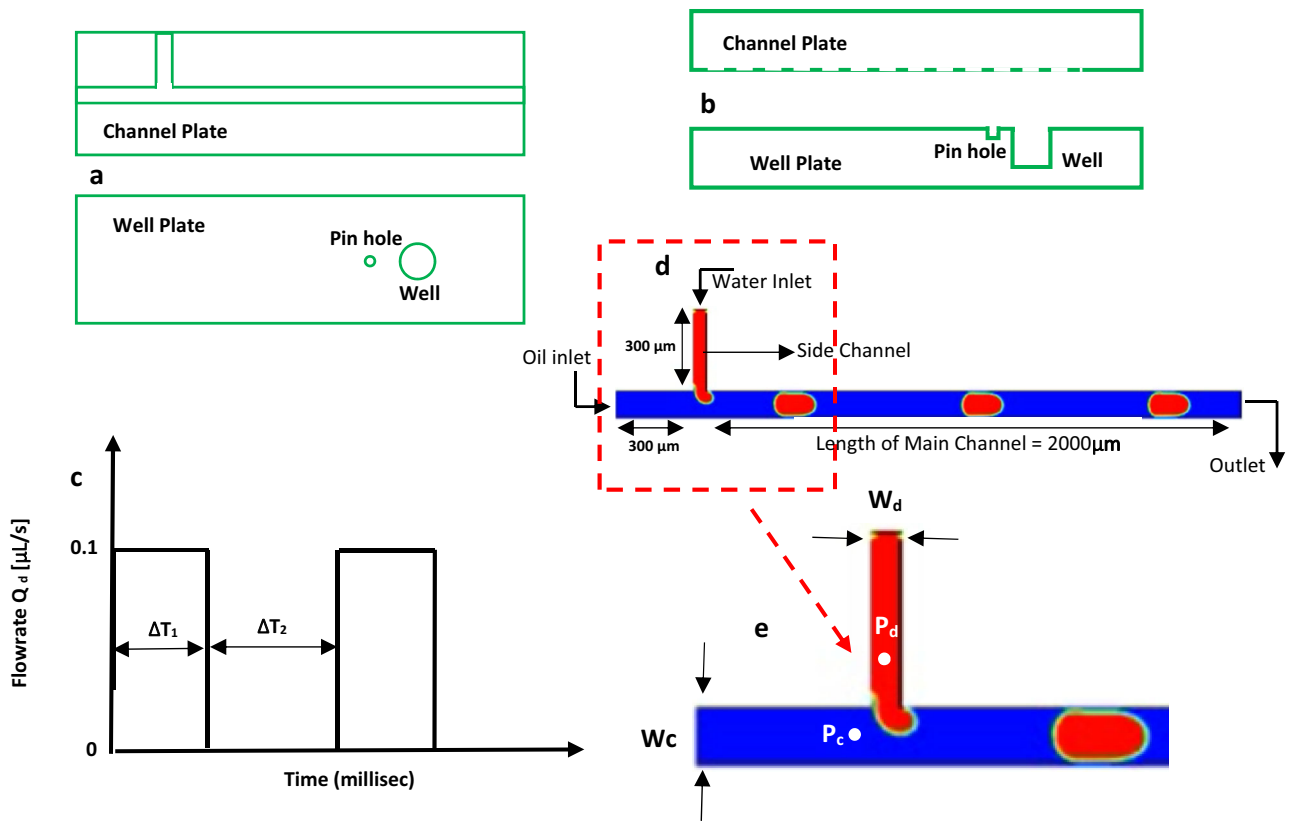
Fig. 1 Schematic of microfluidic device showing the channel and the well: **a** top view and **b** broadside view, **c** representation of pulsed flowrate, **d** 2D device geometry for droplet generation, **e** expanded view of the T-junction device showing the width and pressure measuring points (P_c and P_d)

$$\eta_{\text{avg}} = V_0\eta_o + (1 - V_w)\eta_w \tag{5}$$

where ρ_w, ρ_o are density of and η_w and η_o are the viscosity of water and oil, respectively. The component (V_f) of the particular liquid phase is calculated by solving the below equation.

$$\frac{\partial V_f}{\partial t} + \overrightarrow{U\cdot}\nabla V_f = 0 \tag{6}$$

The subscript "f" in the above equation defines one of the two liquids. In each mesh element, the fractional volume of the two phases is conserved indicating $\Sigma\, V_f = 1$. If $V_f = 0$, the specific mesh element is said to be empty of the fth phase and $V_f = 1$ indicating that the mesh element is loaded with the fth phase. Thus, the two-phase interface is demarcated by the value of the fractional volume.

The continuum surface force (CSF) model is considered and accordingly defines the interfacial tension force ($\overrightarrow{F_{\text{SF}}}$) which is volumetric and is represented as

$$\overrightarrow{F_{\text{SF}}} = \sigma\left(\frac{\rho R_n \nabla V_0}{0.5(\rho_0 + \rho_w)}\right) \tag{7}$$

where "σ" is the coefficient of surface tension between the

two liquids and R_n is the radius of curvature of the droplet which is expressed in terms of

$$R_n = -\nabla \cdot \hat{n} = \frac{1}{|\vec{n}|}\left[\left(\frac{\vec{n}}{|\vec{n}|}\cdot\nabla\right)|\vec{n}| - (\nabla \cdot \vec{n})\right] \tag{8}$$

where $\widehat{n}$ is the component which is normal to the surface of the droplet. In the case of volume-of-fluid (VOF) method, the surface normal $|\overrightarrow{n}|$ is expressed as the gradient of fractional volume phase at the interface, which can be written as

$$\vec{n} = \nabla V_f \tag{9}$$

The surface tension force is implemented by piecewise linear interface calculation (PLIC) (Ranade 2019; Brackbill et al. 1992). The conditions for wall adhesion are considered by feeding the necessary value for the contact angle with the channel wall (Θ_w). Therefore, the surface normal at the reference cell next to the wall is given by,

$$\hat{n} = \hat{n}_w \cos\theta_w + \hat{m}_w \sin\theta_w \tag{10}$$

where $\hat{n}_w$ and $\hat{m}_w$ are the unit vectors which are normal and tangential to the wall respectively.

Mineral oil, used as the continuous phase liquid, flows through the "main channel" of cross section   100 μm x

50 μm (Fig. 1d). Water is used as the dispersed phase liquid, and it flows into the T-junction through the "side channel" of cross section either 50 μm x 50 μm or 25 μm x 50 μm. The length of the main channel is kept 2000 μm from the T-junction to ensure that the droplets acquire a constant shape and size. The microdroplets of water are generated in the main channel and close to the T-junction. The continuous phase liquid, mineral oil, flows at a constant rate in all our simulation studies, whereas the flowrate of the water is pulsed according to the rectangular pulse waveform shown in Fig. 1c. It has been shown that such a rectangular pulse train leads to better control of the droplet size and generation rate (Qian et al. 2019). The water flowrate alternates between 0.1 μl/sec (referred to as on-state) and zero (referred to as off-state). Water enters the main channel in the on-state and does not enter during the off-state. The simulations are carried out for pulse width of $\Delta T_1=6.5$ msec and 3.25 msec and $\Delta T_2=6.5$ msec and 13 msec.

Simulation sequence

Simulations were performed using ANSYS Fluent software v2020 R2 in which the level-set method (LSM) and the volume-of-fluid model (VOF) are used in combination. This combined model has been shown to yield better results than that obtained using VOF alone (Soh et al. 2016).

To compute the coupling effect between the pressure and fluid velocity in the momentum equation, the "Pressure Implicit with Splitting of Operators (PISO)" scheme in ANSYS FLUENT simulation software is used. False currents arising due to the mismatch between pressure and interfacial tension forces were removed using the PREssure STaggering Option (PRESTO). The implicit method of the first order has been adopted for the discretization of time derivatives. The criterion for the convergence of continuity equation, the equations for X-momentum and Y-momentum, and the computation of the level-set function were set as attaining a minimum residual of 0.001. This implies that, during the computation of any residual, if it falls below 0.001; then, the solution is taken to have converged. The flowtime for the computation is set to be 0.1 Sec with a step size of 5 μsec to maintain the global Courant number below 0.2. This ensures that the time-step increment and its duration in the transport equations lead to accurate tracking of transportation of the fluid element across a control volume. The flowrate of the two fluids is specified at the respective inlets, and the normal outflow condition is specified at the common outlet. The length of the droplet generated is noted. Simulations are performed considering the inner surface of the channel wall to be completely wetted by the continuous phase liquid. Hence, the no-slip boundary condition is employed for the continuous phase liquid. Hexahedral mesh elements are adopted. To determine the appropriate size of the mesh element, we computed the droplet length for mesh sizes of 4 μm, 2 μm, and 1 μm. The droplet length changed by less than 1% for mesh size of 2 μm as compared to that for 1 μm. Hence, all the simulations were performed with a mesh element size of 2 μm. The length kept for the microchannel was seen to be adequate for the droplet to be fully developed.

2D simulations are performed for studies pertinent to droplet generation. The surfactant concentration, in terms of the ratio of the weight of Span-80 to that of mineral oil, was kept at 0%, 0.2%, 1%, 2%, and 4%. Droplet generation is studied for an on-state (flowtime) of $\Delta T_1=6.5$ msec and 3.25 msec and off-state (no flowtime) of $\Delta T_2=6.5$ msec and 13 msec, as shown in Fig. 1c. The pressure profiles at point P_d (Fig. 1e) are computed for various surfactant concentrations to get an insight into the droplet generation mechanism. Based on the droplet size generated, we study the trapping mechanism by introducing a small pinhole close to the well in the well plate (Fig. 1b) using 3D simulation. Simulations combining droplet generation and trapping are computationally expensive and intense. Hence, we study droplet generation and trapping mechanisms in two different models. The diameter of the pinhole is varied from 20 μm to 60 μm. The simulation is repeated for a droplet of length 40 μm and diameter of the pinhole from 5 μm to 40 μm, while the depth is fixed to 40 μm.

Results and discussion

We have systematically investigated the generation and trapping of droplets in a T-junction device having a side channel of width $W_d=50$ μm and 25 μm and the main channel of constant width $W_c=100$ μm (Fig. 1d) The droplets are generated by (i) a steady flow of both the liquids and (ii) by pulsed flow of water keeping flowrate of mineral oil fixed. The effect of a small pinhole introduced just before the well, on the trapping of droplets, has also been investigated.

### Droplet generation—Steady flowrate of the two liquids

In the following discussions, we shall denote Device 1 and Device 2 mentioned in Table 1 as D1 and D2. The flowrate Q_d of water is varied such that the flowrate ratio $Q=Q_d/Q_c$ varies from 0.01 to 1; Q_c is the flowrate of mineral oil. In device D1, the length of the droplet decreased gradually from 232 to 94 μm as the flowrate Q_c was increased from 0.06 μl/sec to 2 μl/s, while Q_d is fixed at 0.05 μl/s. In

Table 1 Dimensions of two T-junction devices investigated (see Fig. 1)

Device types	Microchannels	Width (W)	Length (L)	Height (H)
Device 1 (D1)	Side channel	W_d=50 μm	L_d=300 μm	H=50 μm
	Main channel	W_c=100 μm	L_c=2000 μm	
Device 2 (D2)	Side channel	W_d=25 μm	L_d=300 μm	
	Main channel	W_c=100 μm	L_c=2000 μm	

contrast, the droplet length increased from 118 μm to 452 μm when Q_d is increased from 0.003 μl/s to 0.07 μl/s keeping Q_c fixed at 0.05 μl/s. Similarly, in the device D2, the length of the droplet decreased from 256 μm to 80 μm when Q_c was increased from 0.04 μl/s to 2 μl/s, while Q_d was fixed at 0.05 μl/s. The length of the droplet increased from 120 μm to 250 μm when Q_d was increased from 0.003 μl/s to 0.06 μl/s, while Q_c was fixed at 0.05 μl/s. With increasing Q_c, the viscous shear stress is expected to increase, leading to a decrease in droplet length (Fig. 2a). In

On the other hand, an increase in Q_d results in a reduction in the interfacial tension, whereas the viscous shear force does not change much since Q_c is held constant. Consequently, the droplet length increases as shown in Fig. 2b. The variation of dimensionless droplet length with the ratio Q (Fig. 2) is in good agreement with reported experimental results (Garstecki et al. 2006). This validates our simulation results. Our simulations indicate that the droplets are generated in the jetting regime when Q_c is kept constant at 0.05 μl/s and Q_d is kept at a low value of 0.07 μl/s in both
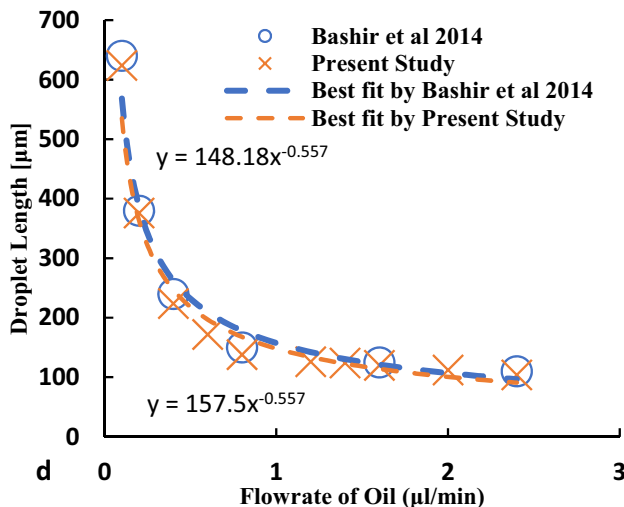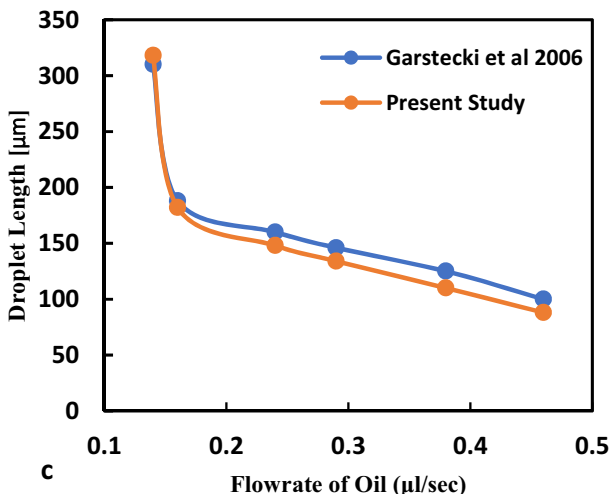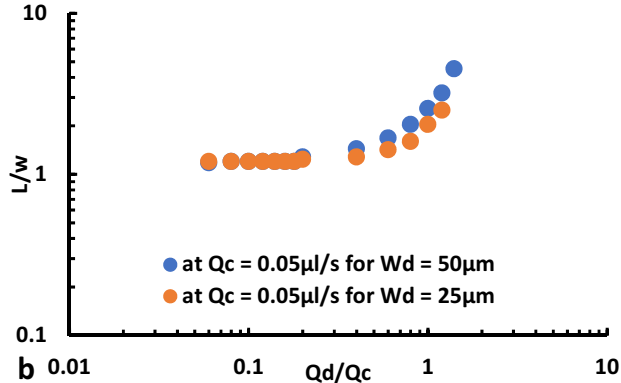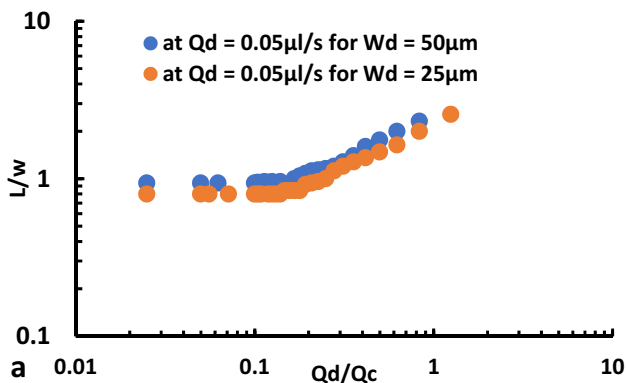
Fig. 2 a Dimensionless length of the droplets (L/w) plotted as a function of the ratio of flowrates (Q_d/Q_c) of fluids a) when Q_d is fixed and Q_c is varied, **b** when Qc is fixed and Q_d is varied. Comparison of droplet length with experimental data reported in the literature for various flowrates of continuous phase liquid (Q_c), **c** Garstecki et al. (2006) (Q_d=0.14 μl/s, η_o=0.01 Pa.s, η_w=0.001 Pa.s and $\overrightarrow{F_{SF}}$ (or γ)= 3.65 mN/m) **d** Bashir et al. (2014) at 2% surfactant concentration. (Q_d=0.2 μl/min)

Table 2 Physical parameters of the two liquids used in the simulations

Liquids used	Viscosity (mPa.s)	Density (Kg/m³)	Flowrate (μl/sec)
Continuous phase liquid (mineral oil)	24.7	840	Q_c=0.04–2.0
Dispersed phase liquid (water)	1	998	Q_d=0.003–0.1

Table 3 Pulsed parameters used in the simulations (see Fig. 1c)

Pulse parameters	Duration (msec)
ΔT_1	6.5 and 3.25
ΔT_2	6.5 and 13

the devices D1 and D2. When Q_d is increased to 0.09 μl/s, the droplet is released farther away from the T-junction. Further increase in Q_d leads to a steady flow of the two liquids, in parallel streams, in the main channel, without the formation of any droplets (Wehking et al. 2014).

The VOF model used in the present study is validated with two different experimental studies done in the past. In the first case, Fig. 2c shows the quantitative comparison of the droplet length estimation with the experimental data as reported by Garstecki et al. (2006). In this case, we have used the same channel dimensions and fluid properties reported by Garstecki et al. (2006) for the study (η_o= 0.01 Pa.s, η_w=0.001 Pa.s and γ=3.65 mN/m). In the second case, fluid properties are as indicated in Table 2 and the channel dimensions are the same as for device D1 (Table 1) except that the width of the side channel is taken as 100 μm. In both cases, the droplet length reduces with an increase in the flowrate of continuous phase liquid.

Droplet generation—Pulsed flow of dispersed phase liquid (water)

In this section, we present simulation results for droplet generation obtained by periodically varying the flowrate (Q_d) of water and keeping the flowrate of mineral oil (Q_c) constant. Experimental results on devices producing droplets on demand as reported in the literature survey show

that, the choice of the flowrate is made based on the results of Droplet generation—Steady flowrate of the two liquids section. As seen in the previous section, droplet generation happens in the jetting regime at low values of Q_d (0.07 μl/s) and parallel flow occurs at higher values of Q_d (0.1 μl/s). In the parallel flow regime, droplets can be generated by increasing Q_c. We see that at Q_c=0.2 μl/s, droplets are generated at the junction. We present the details of this study in Sect. 1 of the supplementary information (SI).
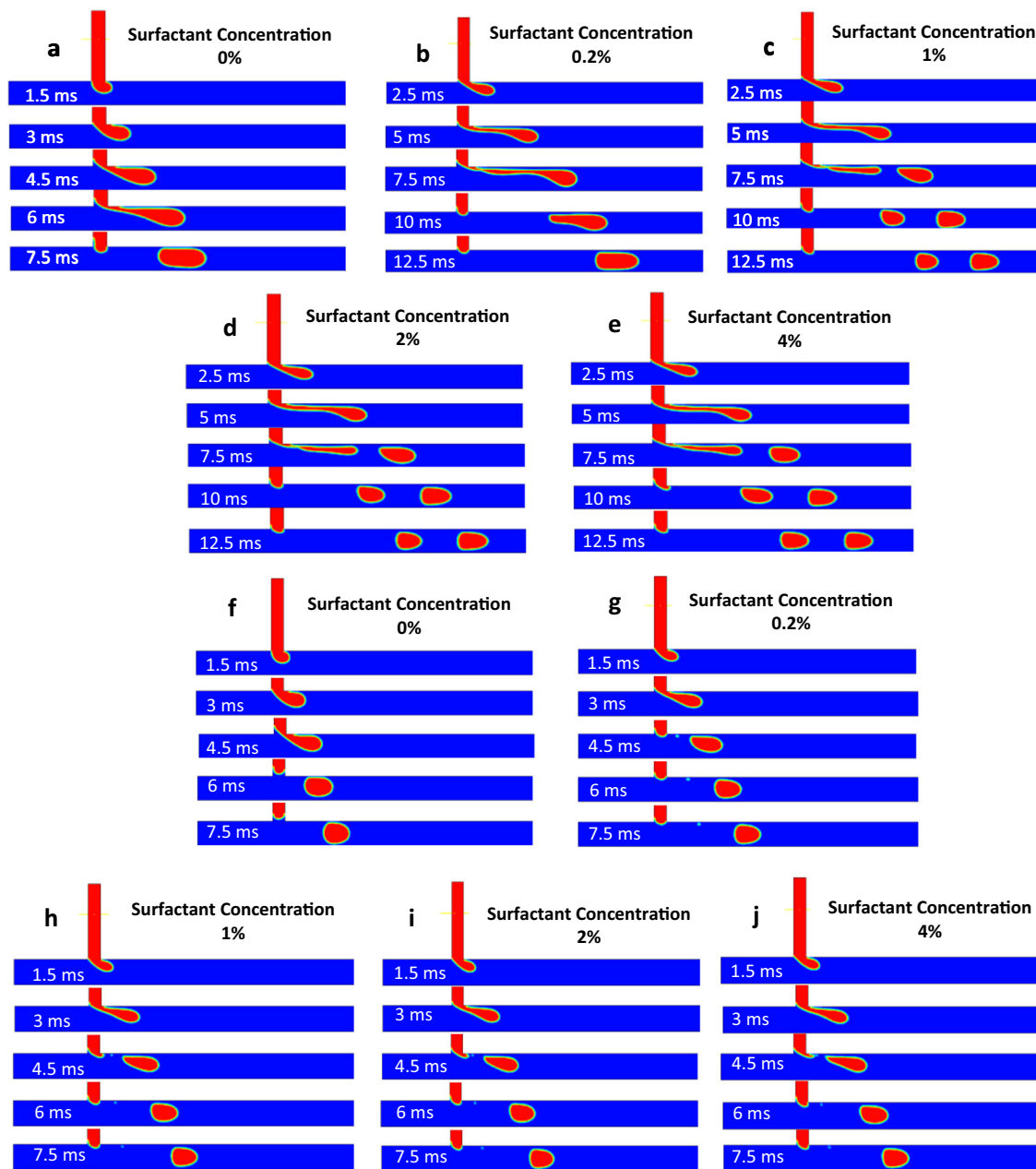
In the simulations, the flowrate Q_c is kept constant at 0.2 μl/s while Q_d is varied between 0.1 μl/s and 0 μl/s. The time interval between two successive droplets was found to be 6.5 msec and 7 msec, respectively, for devices D1 and D2. In the case of D2, the generation of the larger droplets is followed by a few small droplets (called daughter droplets) when the pulse repetition time is kept 7 msec (Flow_7ms_No_Flow_7ms_No_surf.wmv file in SI). Therefore, we studied the droplet generation for pulse parameters shown in Table 3 and for a total simulation duration of 100 msec (Table 4).

Figure 3 shows the successive stages of droplet formation, in device D1, at five instants of time for five different surfactant concentrations. When no surfactant (0%) is added, a single plug-shaped droplet of about 150 μm length is formed close to the T-junction due to the squeezing mechanism. Addition of a small amount (0.2%) of surfactant results in the formation of the droplet (of length $\sim$ 170 μm) further away ($\sim$ 50 μm) from the T-junction (Table 5).

Increasing the surfactant concentration further leads to the formation of two droplets instead of one; the two droplets are also formed well away from the T-junction (Sontti and Atta 2019). This indicates that surfactants reduce the interfacial tension (Bashir et al. 2014), which, in turn, leads to the formation of two smaller droplets, each of

Table 4 Diameter of droplet and pinhole chosen for droplet trapping

Pinhole diameter (μm)	Droplet length (μm)	Pinhole diameter (μm)	Droplet length (μm)
0	80	0	40
20		5	
30		10	
40		15	
45		20	
50		30	
55		40	
60			

Fig. 3 Sequence of droplet generation with and without surfactant for D1; Q_c=0.2 µl/Sec and Q_d=0.1 µl/Sec. **a–e** ΔT_1=6.5 msec and ΔT_2= 6.5 msec, **a** 0%, **b** 0.2%, **c** 1%, **d** 2%, **e** 4%, and **f–j** ΔT_1=3.25 msec and ΔT_2=6.5 msec, **f** 0%, **g** 0.2%, **h** 1%, **i** 2%, **j** 4%

length ~ 100 µm, instead of one large droplet for each pulse cycle. When the on-time pulse duration ΔT_1 is reduced to 3.25 msec, keeping ΔT_2 at 6.5 msec, it is seen that, irrespective of the surfactant concentration, only one droplet of length ~ 100 µm is generated (Fig. 3f–j). Further, the droplets are invariably generated close to the T-junction. This indicated that shorter pulse duration gives better control on the droplet generation and that the use of surfactants is desirable for obtaining smaller droplets.

Pressure variations at points P_c and P_d in the device (Fig. 1e) occur with the same periodicity as the pulse waveform imposed on the flowrate Q_d of the dispersed phase liquid. The graphs in Fig. 4 and Fig. 6 clearly show that the pressure profiles, for the point P_d, are considerably distorted compared to the rectangular waveform for Q_d. The pressure variations at point P_d in the side channel are shown in Fig. 4. It is seen that the pressure in water (dispersed phase liquid) alternates between 4.2 kPa and 3.4 kPa, on average. At each fall time in the graphs shown in Fig. 4a, c for ΔT_1=6.5 msec, an under-shoot is seen which is indicative of droplet release and immediate retraction of water thread into the side channel. If the on-

Table 5 Trapping status of droplet (length 80 μm) based on the flowrate of oil (depth of pinhole is 40 μm)

Diameter of pinhole (μm)	Flowrate of oil (Q_c)			
	0.01 μl/s	0.0125 μl/s	0.015 μl/s	0.02 μl/s
20	Trapped	Trapped	Not trapped	Not trapped
30	Trapped	Not trapped	Not trapped	
40	Trapped	Trapped	Not trapped	
45	Trapped	Trapped	Not trapped	
50	Attached to pinhole	Trapped	Trapped	
55	Attached to pinhole	Trapped	Trapped	
60	Attached to pinhole	Attached to pinhole	Attached to pinhole	

time pulse duration is reduced to $\Delta T_1 = 3.25$ msec, a small step profile is seen just at the fall-time (shown by a circle in Fig. 4e, g). This is seen to indicate the release of the droplet followed by the retraction of the water thread after about 3 msec ($\sim \Delta T_1$).

In contrast, the addition of a surfactant suppresses these variations at the fall-time, thereby implying that the droplet release is immediately followed by retraction of the water thread. This is observed for both values of ΔT_1. Further, the addition of a surfactant leads to a reduction in the average pressure values to 3.5 kPa during on-time and 2.5 kPa during off-time for the pulse (Fig. 4b, d, f, h). *Individual plots of pressure versus time for device D1 is presented, for the sake of clarity, in Sec. 2 of the Supplementary Information.*

The droplet generation process in device D2 is seen to be similar to that in device D1. The length of the droplet produced was found to be 120 μm for $\Delta T_1 = 6.5$ msec and 90 μm for $\Delta T_1 = 3.25$ msec as shown in Fig. 5a, f, respectively. Maintaining the same flowrate for water as in device D1 implied that the flow velocity of water was higher in device D2 as compared to D1 since the width of the side channel in D2 was half that in D1. Due to this reduction in the width of the side channel of device D2, the length of the droplets generated in D2 is smaller than those in D1. Another significant difference is that the generation of a pair of droplets in device D2, for $\Delta T_1 = 6.5$ msec, occurs at a higher concentration (4%) of the surfactant than in D1. As in the case of device D1, for pulses of width $\Delta T_1 = 3.25$ msec, only single droplet is generated in device D2. This confirms the conclusion that smaller pulse width (ΔT_1) leads to better control of droplet generation (Fig. 5f–j).

Figure 6 shows the profiles of pressure in the water at point P_d in device D2. It is seen that the average pressure during the on-state of the pulse is much higher in device D2 than in D1, whereas the pressure during off-state is the same as in D1. This is due to the higher flow velocity caused by the smaller width of the side channel in D2. At

the start of the on-state, a sharp spike in the pressure (~ 5.7 kPa) is seen, which is followed by a minimum and then a steady value (~ 5 kPa) is reached (Fig. 6a, c, e, g). The addition of the surfactant suppresses this variation in pressure, and it is seen to reduce gradually from a maximum value (~ 4.2 kPa) at the start of the on-state to a lower value (~ 3.8 kPa) at the end of the on-state of the pulse.

The pressure at point P_d in the off-time of the pulse is seen to reduce from ~ 3 kPa to ~ 2.5 kPa as the surfactant concentration is increased from zero to 4% (Piccin et al. 2014). This is shown in Fig. 6b, d, f, h. The pressure variation in the off-state indicates that the droplet is released at the pulse fall-time instant, and the retraction of the water thread back into the side channel follows immediately without any time gap. These results reveal that the effect of surfactants is stronger in device D2. Thus, the control on droplet generation is better with a side channel of width smaller than the main channel by a factor of about 0.25. *Individual plots of pressure versus time for device D2 is presented, for the sake of clarity, in Sec.3 of the Supplementary Information.*
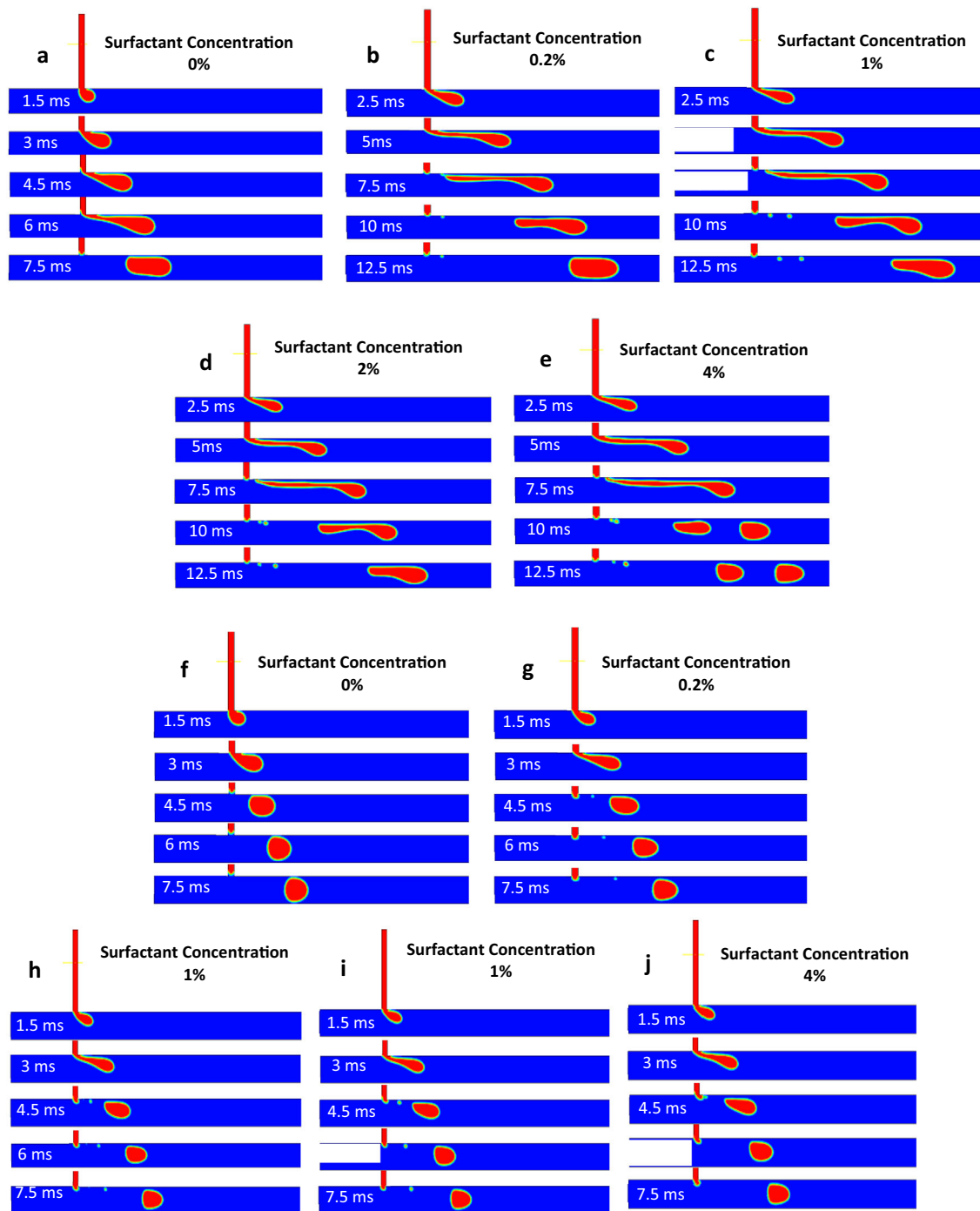
Droplet trapping

The generated droplets are generally collected in a vial, or it is trapped in a microwell assay (Shi et al. 2013). In our previous work, we have shown that trapping of droplets in a microwell occurs if the flow velocity of the continuous phase liquid is less than a critical velocit. Trapping is also assisted by the presence of a circular Pit, located just above the well. In the present work, we have adopted a simpler geometry as indicated in Fig. 1a, b wherein a small pinhole is placed close to the well. Our simulations indicate that the depth of the pinhole does not affect the trapping of droplets. Hence, the depth of the pinhole is fixed at 40 μm, whereas the diameter is varied.
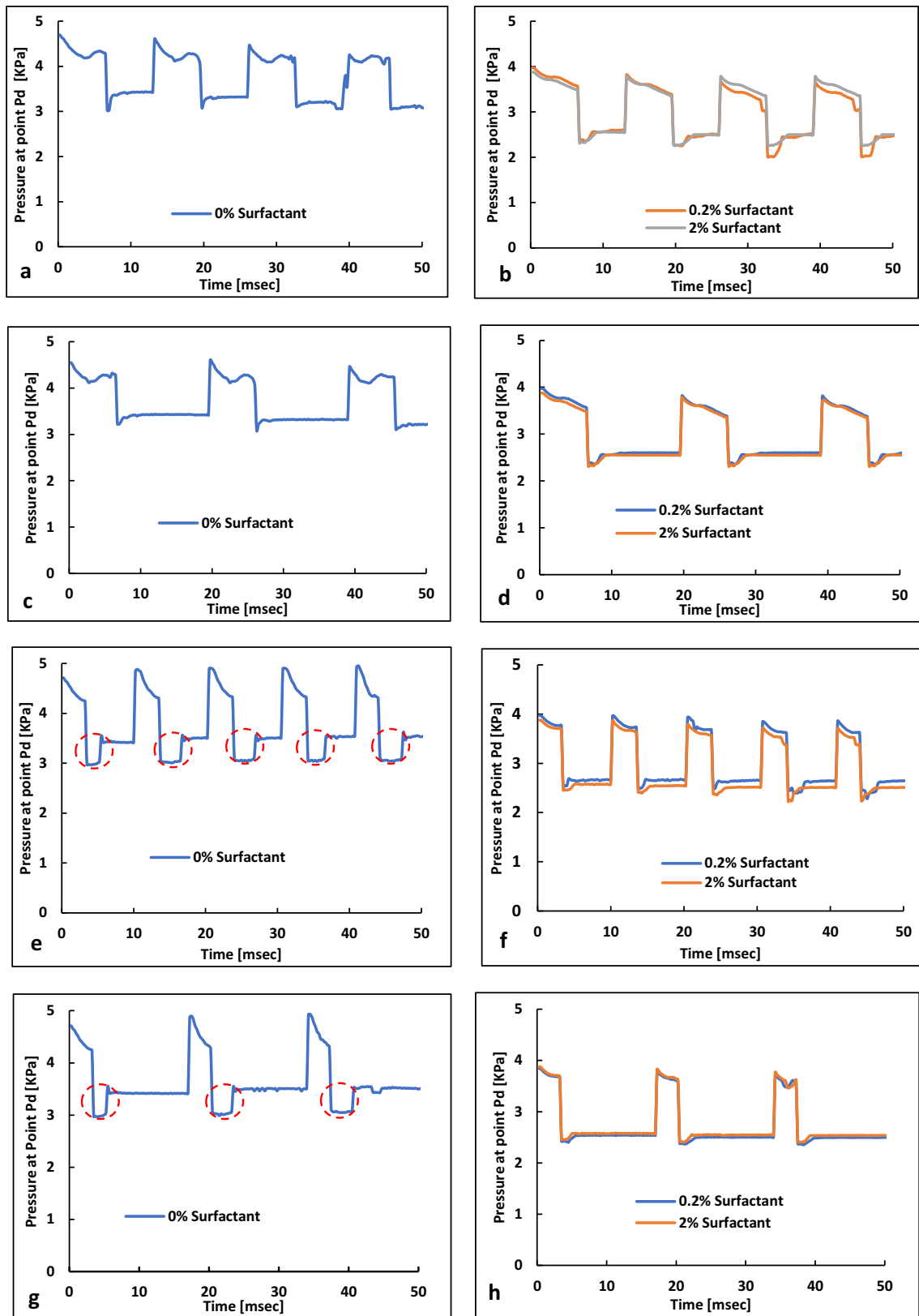
Fig. 4 Pressure versus time at point Pd for D1 with and without surfactant. **a, b** $\Delta T1 = \Delta T2 = 6.5$ msec, **c, d** $\Delta T1 = 6.5$ msec and $\Delta T2 = 13$ msec, **e, f** $\Delta T1 = 3.25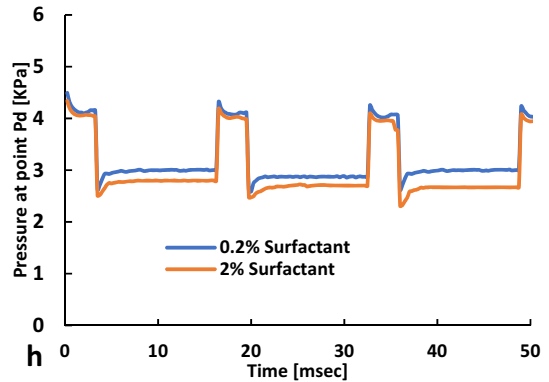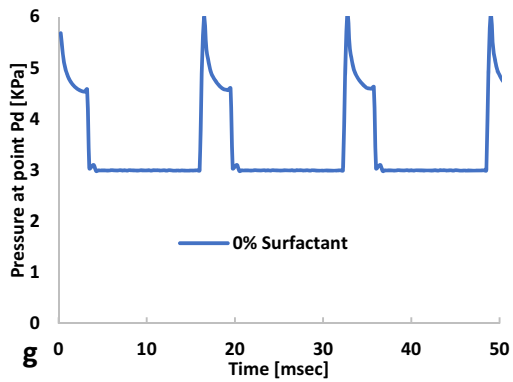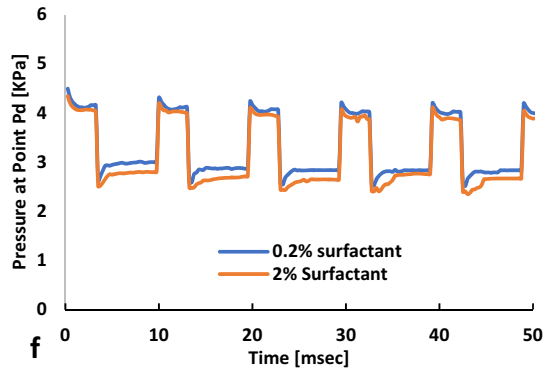$ msec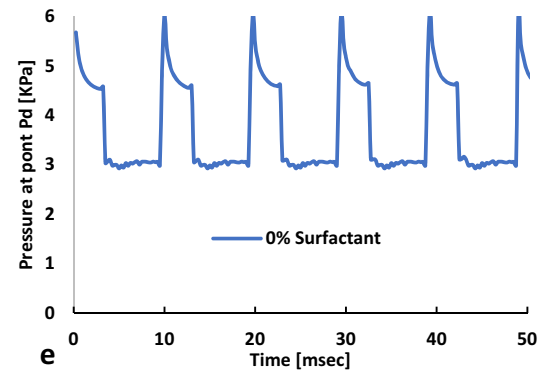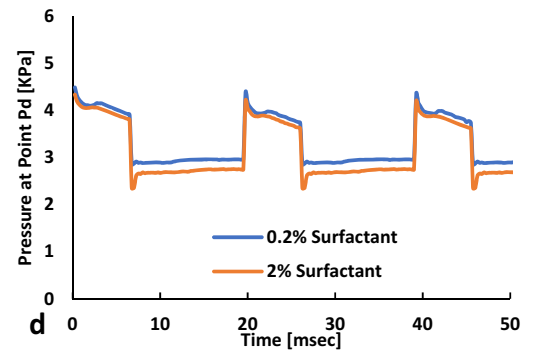 and $\Delta T2 = 6.5$ msec, **g, h** $\Delta T1 = 3.25$ msec and $\Delta T2 = 13$ msec. Operating flowrates are $Qd = 0.1$ μl/s (ON state), 0 μl/s (OFF state) and $Qc = 0.2$ μl/s

Fig. 5 Sequence of droplet generation with and without surfactant for D2; Q_c=0.2 µl/Sec and Q_d=0.1 µl/Sec. **a–e** ΔT_1=6.5 msec and ΔT_2= 6.5 msec, **a** 0%, **b** 0.2%, **c** 1%, **d** 2%, **e** 4%, and **f–j** ΔT_1=3.25 msec and ΔT_2=6.5 msec, **f** 0%, **g** 0.2%, **h** 1%, **i** 2%, **j** 4%

We have simulated the trapping of water droplets of length 40 µm in a well of diameter 200 µm and depth 200 µm. The pinhole depth is kept 40 µm in all the simulations, but its diameter is varied from 5 µm to 40 µm. It is seen that such droplets get trapped in the well for Q_c= 0.01 µl/s and for pinhole diameters in the range of 5 µm– 15 µm. At higher pinhole diameters, the droplet gets attached to the pinhole itself and does not move further. The droplet gets trapped in the absence of the pinhole. If Q_c is further increased to 0.02 µl/s, no trapping of the droplet is seen for pinhole diameter in the entire range of 20 µm– 60 µm. If a surfactant is added to the mineral oil at 0.05% concentration, the droplets do not get trapped even for Q_c= 0.01 µl/s.
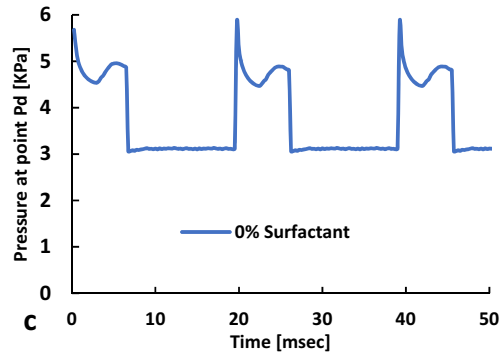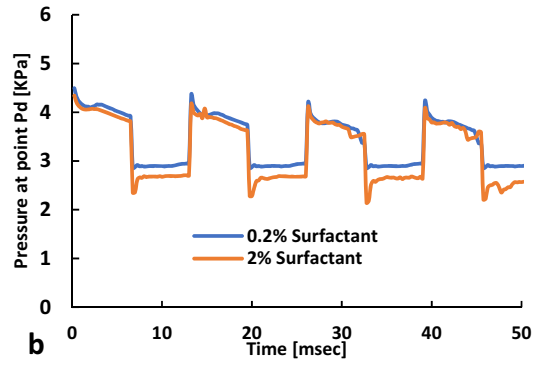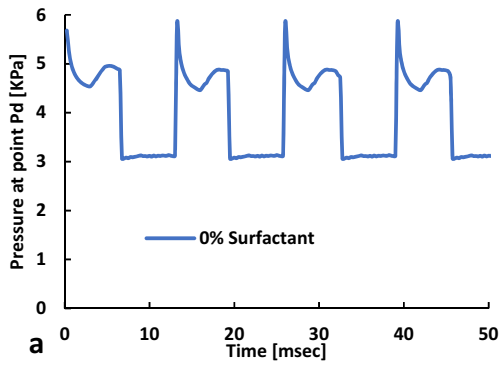
◄**Fig. 6** Pressure versus time at point P_d for D2 with and without surfactant. **a, b** $\Delta T_1 = \Delta T_2 = 6.5$ msec, **c, d** $\Delta T_1 = 6.5$ msec and $\Delta T_2 = 13$ msec, **e, f** $\Delta T_1 = 3.25$ msec and $\Delta T_2 = 6.5$ msec, **g, h** $\Delta T_1 = 3.25$ msec and $\Delta T_2 = 13$ msec. Operating flowrates are $Q_d = 0.1$ μl/s (ON state), 0 μl/s (OFF state) and $Q_c = 0.2$ μl/s

We have also studied trapping of droplets of length 80 μm, keeping $Q_d = 0.05$ μl/s and varying Q_c. The pinhole diameter is also varied from 20 μm to 60 μm, and its depth is kept fixed at 40 μm. It is seen that at $Q_c = 0.01$ μl/s the droplet gets trapped in the well for pinhole diameter< 50 μm, and at higher pinhole diameters the droplet stays attached to the pinhole. If Qc is increased to 0.0125 μl/s, the droplet does not get trapped for pinhole diameter< 45 μm. Trapping of the droplet occurs for pinhole diameter in the range of 50 μm–55 μm. At a higher pinhole diameter, the droplet gets attached to the pinhole. In the absence of a pinhole, no trapping of the droplet is seen. If Qc is further increased to 0.02 μl/s, no trapping is observed. No trapping of the droplets is seen if a surfactant is added at a concentration of 0.05%. Thus, the larger droplet shows a behavior similar to that of the smaller droplet. *For more information, refer to the videos in the folder "trapping" in the supplementary information.*

Therefore, we conclude that droplet trapping is seen to occur only for optimum values of pinhole diameter and Q_c less than 0.02 μl/s. Our simulations also show that if the pinhole is removed from the device, the droplets do not get trapped in the well for the entire range of parameters used in our simulations. Thus, the pinhole is clearly seen to facilitate trapping the microdroplets.

Conclusion

We have investigated the generation and trapping of droplets in a T-junction microfluidic device. The scaling of droplet length with the increase in the flowrate of continuous phase liquid is in good agreement with reported experimental data done in the past. When the droplets are generated by pulsing the dispersed phase liquid between zero and 0.1 μl/s (on-time=6.5 msec), a pair of droplets are generated when surfactant is added at surfactant concentration of 1% in the case of device D1 and at 4% in the case of device D2. The average pressure between on and off states at point P_d switches between 4.2 kPa and 3.4 kPa in the case of D1 and between 5 kPa and 3 kPa in the case of D2. This average pressure reduces with the addition of surfactant. A single droplet is generated when the pulse duration is reduced (on-time=3.25 ms) irrespective of surfactant concentration. In this case, a small step profile is seen just after the fall time, which clearly indicates the

release of the droplet followed by the retraction of the water thread into the side channel over a small-time duration. This time duration for the retraction of water reduces drastically with the addition of surfactant.

A small pinhole ahead of the microwell aids in trapping the microdroplet. Droplets of length 80 μm get trapped in the microwell when $Qc \leq 0.01$ μl/sec for pinhole diameter from 20 to 50 μm. At $Q_c = 0.0125$ μl/sec, the trapping of the droplet is seen for pinhole diameter between 45 μm and 55 μm. In the case of droplets of length 40 μm, trapping of the droplet is seen when $Q_c = 0.01$ μl/sec for the diameter of pinhole< 20 μm. When a surfactant is added, no trapping of droplets is seen. Our simulations clearly indicate microdroplets can be generated in a controlled manner, by pulsed flow technique, and trapped in microwells in microfluidic devices.

Declaration

References

Abbyad P, Dangla R, Alexandrou A, Baroud CN (2011) Rails and anchors: guiding and trapping droplet microreactors in two dimensions. Lab Chip 11:813–821. https://doi.org/10.1039/C0LC00104J

Amselem G, Brun PT, Gallaire F, Baroud CN (2015) Breaking anchored droplets in a microfluidic Hele-Shaw cell. Phys Rev Applied 3:054006. https://doi.org/10.1103/PhysRevApplied.3.054006

Babahosseini H, Misteli T, DeVoe DL (2019) Microfluidic on-demand droplet generation, storage, retrieval, and merging for single-cell pairing. Lab Chip 19:493–502. https://doi.org/10.1039/C8LC01178H

Bashir S, Rees JM, Zimmerman WB (2011) Simulations of microfluidic droplet formation using the two-phase level set method. Chem Eng Sci 66:4733–4741. https://doi.org/10.1016/j.ces.2011.06.034

Bashir S, Solvas XCi, Bashir M, Rees JM, Zimmerman WBJ (2014) Dynamic wetting in microfluidic droplet formation. BioChip J 8:122–128. https://doi.org/10.1007/s13206-014-8207-y

Bastani D, Fayzi P, Lotfi M, Arzideh SM (2018) CFD simulation of bubble in flow field: investigation of dynamic interfacial behaviour in presence of surfactant molecules. Colloid Interface Sci Commun 27:1–10. https://doi.org/10.1016/j.colcom.2018.09.001

Batchelor GK (2000) An introduction to fluid dynamics. Cambridge University Press, Cambridge

Beneyton T, Wijaya IPM, Postros P, Najah M, Leblond P, Couvent A, Mayot E, Griffiths AD, Drevelle A (2016) High-throughput

screening of filamentous fungi using nanoliter-range droplet-based microfluidics. Sci Rep 6:1–10. https://doi.org/10.1038/srep27223

Brackbill JU, Kothe DB, Zemach C (1992) A continuum method for modeling surface tension. J Comput Phys 100:335–354. https://doi.org/10.1016/0021-9991(92)90240-Y

Brouzes E, Medkova M, Savenelli N, Marran D, Twardowski M, Hutchison JB, Rothberg JM, Link DR, Perrimon N, Samuels ML (2009) Droplet microfluidic technology for single-cell high-throughput screening. PNAS 106:14195–14200. https://doi.org/10.1073/pnas.0903542106

Carrier O, Funfschilling D, Li HZ (2014) Effect of the fluid injection configuration on droplet size in a microfluidic T junction. Phys Rev E 89:013003. https://doi.org/10.1103/PhysRevE.89.013003

Chen S, Liu K, Liu C, Wang D, Ba D, Xie Y, Du G, Ba Y, Lin Q (2016) Effects of surface tension and viscosity on the forming and transferring process of microscale droplets. Appl Surf Sci 388:196–202. https://doi.org/10.1016/j.apsusc.2016.01.205

Chiarello E, Gupta A, Mistura G, Sbragaglia M, Pierno M (2017) Droplet breakup driven by shear thinning solutions in a microfluidic T-junction. Phys Rev Fluids 2:123602. https://doi.org/10.1103/PhysRevFluids.2.123602

Christopher GF, Noharuddin NN, Taylor JA, Anna SL (2008) Experimental observations of the squeezing-to-dripping transition in T-shaped microfluidic junctions. Phys Rev E 78:036317. https://doi.org/10.1103/PhysRevE.78.036317

Churski K, Michalski J, Garstecki P (2010) Droplet on demand system utilizing a computer controlled microvalve integrated into a stiff polymeric microfluidic device. Lab Chip 10:512–518. https://doi.org/10.1039/B915155A

Collins DJ, Neild A, deMello A, Liu A-Q, Ai Y (2015) The Poisson distribution and beyond: methods for microfluidic droplet production and single cell encapsulation. Lab Chip 15:3439–3459. https://doi.org/10.1039/C5LC00614G

Dangla R, Lee S, Baroud CN (2011) Trapping microfluidic drops in wells of surface energy. Phys Rev Lett 107:124501. https://doi.org/10.1103/PhysRevLett.107.124501

Datta SS, Abbaspourrad A, Amstad E, Fan J, Kim S-H, Romanowsky M, Shum HC, Sun B, Utada AS, Windbergs M, Zhou S, Weitz DA (2014) 25th anniversary article: double emulsion templated solid microcapsules—mechanics and controlled release. Adv Mater 26:2205–2218. https://doi.org/10.1002/adma.201305119

Garstecki P, Fuerstman MJ, Stone HA, Whitesides GM (2006) Formation of droplets and bubbles in a microfluidic T-junction—scaling and mechanism of break-up. Lab Chip 6:437–446. https://doi.org/10.1039/B510841A

Glawdel T, Ren CL (2012) Droplet formation in microfluidic T-junction generators operating in the transitional regime. III. Dynamic surfactant effects. Phys Rev E 86:026308. https://doi.org/10.1103/PhysRevE.86.026308

Guo F, Liu K, Ji X-H, Ding H-J, Zhang M, Zeng Q, Liu W, Guo S-S, Zhao X-Z (2010) Valve-based microfluidic device for droplet on-demand operation and static assay. Appl Phys Lett 97:233701. https://doi.org/10.1063/1.3521283

Gupta A, Kumar R (2010) Flow regime transition at high capillary numbers in a microfluidic T-junction: viscosity contrast and geometry effect. Phys Fluids 22:122001. https://doi.org/10.1063/1.3523483

Gupta A, Matharoo HS, Makkar D, Kumar R (2014) Droplet formation via squeezing mechanism in a microfluidic flow-focusing device. Comput Fluids 100:218–226. https://doi.org/10.1016/j.compfluid.2014.05.023

Hong Y, Wang F (2007) Flow rate effect on droplet control in a co-flowing microfluidic device. Microfluid Nanofluid 3:341–346. https://doi.org/10.1007/s10404-006-0134-3

Jakiela S, Debski PR, Dabrowski B, Garstecki P (2014) Generation of nanoliter droplets on demand at hundred-Hz frequencies. Micromachines 5:1002–1011. https://doi.org/10.3390/mi5041002

Kemna EWM, Schoeman RM, Wolbers F, Vermes I, Weitz DA, van den Berg A (2012) High-yield cell ordering and deterministic cell-in-droplet encapsulation using Dean flow in a curved microchannel. Lab Chip 12:2881–2887. https://doi.org/10.1039/C2LC00013J

Kong T, Wu J, Yeung KWK, To MKT, Shum HC, Wang L (2013) Microfluidic fabrication of polymeric core-shell microspheres for controlled release applications. Biomicrofluidics 7: 044128. https://doi.org/10.1063/1.4819274

Lee TY, Choi TM, Shim TS, Frijns RAM, Kim S-H (2016) Microfluidic production of multiple emulsions and functional microcapsules. Lab Chip 16:3415–3440. https://doi.org/10.1039/C6LC00809G

Li X-B, Li F-C, Yang J-C, Kinoshita H, Oishi M, Oshima M (2012) Study on the mechanism of droplet formation in T-junction microchannel. Chem Eng Sci 69:340–351. https://doi.org/10.1016/j.ces.2011.10.048

Li X, He L, He Y, Gu H, Liu M (2019) Numerical study of droplet formation in the ordinary and modified T-junctions. Phys Fluids 31:082101. https://doi.org/10.1063/1.5107425

Lin B-C, Su Y-C (2008) On-demand liquid-in-liquid droplet metering and fusion utilizing pneumatically actuated membrane valves. J Micromech Microeng 18:115005. https://doi.org/10.1088/0960-1317/18/11/115005

Liu H, Zhang Y (2009) Droplet formation in a T-shaped microfluidic junction. J Appl Phys 106:034906. https://doi.org/10.1063/1.3187831

Liu H, Zhang Y (2017) Lattice Boltzmann simulation of the trapping of a microdroplet in a well of surface energy. Comput Fluids 155:68–75. https://doi.org/10.1016/j.compfluid.2016.10.031

Liu Z, Zhao J, Pang Y, Wang X (2018) Generation of droplets in the T-junction with a constriction microchannel. Microfluid Nanofluid 22:124. https://doi.org/10.1007/s10404-018-2144-3

Loizou K, Wong V-L, Hewakandamby B (2018) Examining the effect of flow rate ratio on droplet generation and regime transition in a microfluidic T-junction at constant capillary numbers. Inventions 3:54. https://doi.org/10.3390/inventions3030054

Menech MD, Garstecki P, Jousse F, Stone HA (2008) Transition from squeezing to dripping in a microfluidic T-shaped junction. J Fluid Mech 595:141–161. https://doi.org/10.1017/S002211200700910X

Nagel M, Brun P-T, Gallaire F (2014) A numerical study of droplet trapping in microfluidic devices. Phys Fluids 26:032002. https://doi.org/10.1063/1.4867251

Nekouei M, Vanapalli SA (2017) Volume-of-fluid simulations in microfluidic T-junction devices: influence of viscosity ratio on droplet size. Phys Fluids 29:032007. https://doi.org/10.1063/1.4978801

Nunes JK, Tsai SSH, Wan J, Stone HA (2013) Dripping and jetting in microfluidic multiphase flows applied to particle and fiber synthesis. J Phys D Appl Phys. https://doi.org/10.1088/0022-3727/46/11/114002

Peng L, Yang M, Guo S, Liu W, Zhao X (2011) The effect of interfacial tension on droplet formation in flow-focusing microfluidic device. Biomed Microdevices 13:559–564. https://doi.org/10.1007/s10544-011-9526-6

Piccin E, Ferraro D, Sartori P, Chiarello E, Pierno M, Mistura G (2014) Generation of water-in-oil and oil-in-water microdroplets in polyester-toner microfluidic devices. Sens Actuators B Chem 196:525–531. https://doi.org/10.1016/j.snb.2014.02.042

Qian JY, Chen M, Wu Z, Jin Z, Sunden B (2019) Effects of a dynamic injection flow rate on slug generation in a cross-junction square

microchannel. Processes 7:765. https://doi.org/10.3390/pr7100765

Ranade V (2019) Computational flow modeling for chemical reactor engineering, Volume 5—1st Edition. https://www.elsevier.com/books/computational-flow-modeling-for-chemical-reactor-engineering/ranade/978-0-12-576960-0. Accessed 24 Nov 2019

Riaud A, Zhang H, Wang X, Wang K, Luo G (2018) Numerical study of surfactant dynamics during emulsification in a T-junction microchannel. Langmuir. https://doi.org/10.1021/acs.langmuir.8b00123

Seo M, Paquet C, Nie Z, Xu S, Kumacheva E (2007) Microfluidic consecutive flow-focusing droplet generators. Soft Matter 3:986–992. https://doi.org/10.1039/B700687J

Shi Y, Gao X, Chen L, Zhang M, Ma J, Zhang X, Qin J (2013) High throughput generation and trapping of individual agarose microgel using microfluidic approach. Microfluid Nanofluid 15:467–474. https://doi.org/10.1007/s10404-013-1160-6

Simon MG, Lin R, Fisher JS, Lee AP (2012) A Laplace pressure based microfluidic trap for passive droplet trapping and controlled release. Biomicrofluidics 6:014110. https://doi.org/10.1063/1.3687400

Soh GY, Yeoh GH, Timchenko V (2016) Improved volume-of-fluid (VOF) model for predictions of velocity fields and droplet lengths in microchannels. Flow Meas Instrum 51:105–115. https://doi.org/10.1016/j.flowmeasinst.2016.09.004

Song H, Li H-W, Munson MS, Van Ha TG, Ismagilov RF (2006) On-chip titration of an anticoagulant argatroban and determination of the clotting time within whole blood or plasma using a plug-based microfluidic system. Anal Chem 78:4839–4849. https://doi.org/10.1021/ac0601718

Sontti SG, Atta A (2017) CFD analysis of microfluidic droplet formation in non–Newtonian liquid. Chem Eng J 330:245–261. https://doi.org/10.1016/j.cej.2017.07.097

Sontti SG, Atta A (2019) CFD study on Taylor bubble characteristics in Carreau-Yasuda shear thinning liquids. Can J Chem Eng 97:616–624. https://doi.org/10.1002/cjce.23311

Sun X, Tang K, Smith RD, Kelly RT (2013) Controlled dispensing and mixing of pico- to nanoliter volumes using on-demand droplet-based microfluidics. Microfluid Nanofluid 15:117–126. https://doi.org/10.1007/s10404-012-1133-1

Tadros TF (2013) Emulsion formation, stability, and rheology. In: Emulsion formation and stability. John Wiley & Sons, Ltd, pp 1–75

Tangen U, Sharma A, Wagler P, McCaskill JS (2015) On demand nanoliter-scale microfluidic droplet generation, injection, and mixing using a passive microfluidic device. Biomicrofluidics 9:014119. https://doi.org/10.1063/1.4907895

Thorsen T, Roberts RW, Arnold FH, Quake SR (2001) Dynamic pattern formation in a vesicle-generating microfluidic device. Phys Rev Lett 86:4163–4166. https://doi.org/10.1103/PhysRevLett.86.4163

Totlani K, Hurkmans J-W, van Gulik WM, Kreutzer MT, van Steijn V (2020) Scalable microfluidic droplet on-demand generator for non-steady operation of droplet-based assays. Lab Chip 20:1398–1409. https://doi.org/10.1039/C9LC01103J

Wang W, Yang C, Li CM (2009) On-demand microfluidic droplet trapping and fusion for on-chip static droplet assays. Lab Chip 9:1504–1506. https://doi.org/10.1039/B903468D

Wehking JD, Gabany M, Chew L, Kumar R (2014) Effects of viscosity, interfacial tension, and flow geometry on droplet formation in a microfluidic T-junction. Microfluid Nanofluid 16:441–453. https://doi.org/10.1007/s10404-013-1239-0

Yan Y, Guo D, Wen SZ (2012) Numerical simulation of junction point pressure during droplet formation in a microfluidic T-junction. Chem Eng Sci 84:591–601. https://doi.org/10.1016/j.ces.2012.08.055

Yang H, Zhou Q, Fan L-S (2013) Three-dimensional numerical study on droplet formation and cell encapsulation process in a micro T-junction. Chem Eng Sci 87:100–110. https://doi.org/10.1016/j.ces.2012.10.008

Zec H, Rane TD, Wang T-H (2012) Microfluidic platform for on-demand generation of spatially indexed combinatorial droplets. Lab Chip 12:3055–3062. https://doi.org/10.1039/C2LC40399D

Zhang Y, Jiang H-R (2016) A review on continuous-flow microfluidic PCR in droplets: advances, challenges and future. Anal Chim Acta 914:7–16. https://doi.org/10.1016/j.aca.2016.02.006

Zheng B, Tice JD, Roach LS, Ismagilov RF (2004) A droplet-based, composite PDMS/glass capillary microfluidic system for evaluating protein crystallization conditions by microbatch and vapor-diffusion methods with on-chip X-ray diffraction. Angew Chem Int Ed 43:2508–2511. https://doi.org/10.1002/anie.200453974